JACS
JOURNAL OF THE AMERICAN CHEMICAL SOCIETY

ARTICLE

pubs.acs.org/JACS

Photocatalytic Hydrogen Evolution under Highly Basic Conditions by Using Ru Nanoparticles and 2-Phenyl-4-(1-naphthyl)quinolinium Ion

Yusuke Yamada,[†] Takamitsu Miyahigashi,[†] Hiroaki Kotani,[†] Kei Ohkubo,[†] and Shunichi Fukuzumi*[,†,‡]

[†]Department of Material and Life Science, Graduate School of Engineering, Osaka University, and ALCA, Japan Science and Technology Agency (JST), Suita, Osaka 565-0871, Japan

[‡]Department of Bioinspired Science, Ewha Womans University, Seoul 120-750, Korea

Supporting Information

ABSTRACT: Photocatalytic hydrogen evolution with a ruthenium metal catalyst under basic conditions (pH 10) has been made possible for the first time by using 2-phenyl-4-(1-naphthyl)-quinolinium ion ($QuPh^+$—NA), dihydronicotinamide adenine dinucleotide (NADH), and Ru nanoparticles (RuNPs) as the photocatalyst, electron donor, and hydrogen-evolution catalyst, respectively. The catalytic reactivity of RuNPs was virtually the same as that of commercially available PtNPs. Nanosecond laser flash photolysis measurements were performed to examine the photodynamics of $QuPh^+$—NA in the presence of NADH. Upon photoexcitation of $QuPh^+$—NA, the electron-transfer state of $QuPh^+$—NA ($QuPh^{\bullet}$—$NA^{\bullet+}$) is produced, followed by formation of the π-dimer radical cation with $QuPh^+$—NA, [($QuPh^{\bullet}$—$NA^{\bullet+}$)($QuPh^+$—NA)]. Electron transfer from NADH to the π-dimer radical cation leads to the production of 2 equiv of $QuPh^{\bullet}$—NA via deprotonation of $NADH^{\bullet+}$ and subsequent electron transfer from $NAD^{\bullet}$ to $QuPh^+$—NA. Electron transfer from the photogenerated $QuPh^{\bullet}$—NA to RuNPs results in hydrogen evolution even under basic conditions. The rate of electron transfer from $QuPh^{\bullet}$—NA to RuNPs is much higher than the rate of hydrogen evolution. The effect of the size of the RuNPs on the catalytic reactivity for hydrogen evolution was also examined by using size-controlled RuNPs. RuNPs with a size of 4.1 nm exhibited the highest hydrogen-evolution rate normalized by the weight of RuNPs.

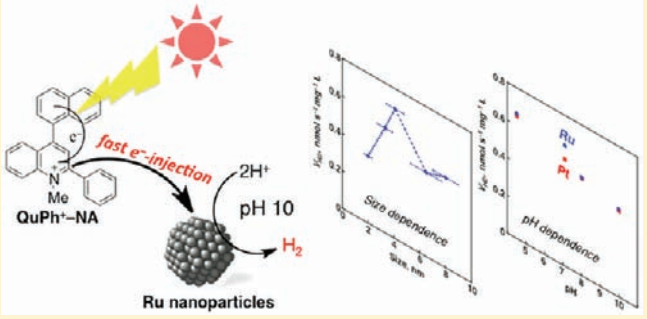

INTRODUCTION

Hydrogen is regarded as a clean fuel of the next generation to reduce consumption of fossil fuels and emission of greenhouse gases.[1] Most hydrogen supplied for industries is produced from fossil fuels such as methane by the steam-reforming reaction at high temperature followed by the water—gas shift reaction with emission of carbon dioxide, which is regarded as a typical greenhouse gas.[2] In order to reduce the carbon dioxide emission, the most promising method is hydrogen production from water utilizing solar energy.[3] In the past few decades, extensive efforts have been devoted to the development of various photocatalytic hydrogen-evolution systems consisting of a sacrificial electron donor, a photosensitizer, an electron mediator, and a hydrogen-evolution catalyst.[4−12] The photocatalytic efficiency of hydrogen evolution has been improved by using a donor—acceptor-linked molecule with a long-lived charge-separated state, which can inject electrons directly into the hydrogen-evolution catalyst without an electron mediator upon photoexcitation of the donor—acceptor-linked dyads.[13]

The most efficient catalyst used to date for hydrogen evolution is Pt nanoparticles (PtNPs), because Pt has a low overpotential for proton reduction to evolve hydrogen.[14] However, avoiding the use of Pt metal is strongly desired because of its high cost and limited supply. Thus, development of hydrogen-evolution catalysts composed of inexpensive and abundant metals has merited considerable interest.[15−18] In biological systems, hydrogen production is exclusively based on the enzymatic reactivity of hydrogenases containing no precious metals.[19−22] Hydrogenases are capable of catalyzing the reversible reaction $2H^+ + 2e^- \rightleftarrows H_2$ using base metals (predominantly Fe and Ni) at their catalytic sites.[23,24] Hydrogenases have been successfully utilized as hydrogen-evolution catalysts for constructing artificial hydrogen-evolution systems.[25−28] Fe nanoparticles (FeNPs) have recently been utilized as the hydrogen-evolution catalyst in a photocatalytic system with a long-lived charge-separation molecule without an electron mediator.[29] However, the catalytic efficiency for hydrogen evolution with FeNPs was much lower than that with PtNPs.[20]

Photocatalytic hydrogen evolution with sacrificial electron donors has so far been performed under neutral to acidic conditions, where hydrogen evolution is thermodynamically favorable.[30] In order to replace sacrificial electron donors by water, it is highly desired to develop a hydrogen-evolution system working under basic conditions, because water oxidation under basic conditions

Received: June 30, 2011
Published: August 29, 2011

dx.doi.org/10.1021/ja206079e | J. Am. Chem. Soc. 2011, 133, 16136–16145

Scheme 1. Structure of $QuPh^+$—NA and the Overall Catalytic Cycle for Photocatalytic Hydrogen Evolution Using $QuPh^+$—NA and Metal Nanoparticles (MNPs, M = Ru, Pt, Fe)

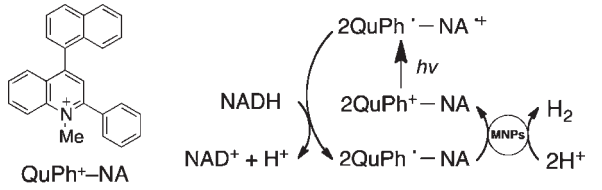

is thermodynamically more favorable than that under acidic conditions.[31] Some hydrogen-evolution systems using Pt catalysts have been reported to evolve hydrogen under basic conditions,[10] but photocatalytic hydrogen evolution with non-Pt metal particles under highly basic conditions has yet to be achieved.

We report herein a photocatalytic hydrogen-evolution system that uses Ru nanoparticles (RuNPs) and PtNPs as hydrogen-evolution catalysts under highly basic conditions (pH ~10). This is the first time that efficient photocatalytic hydrogen evolution with Ru metal particles under highly basic conditions has been achieved and also the first demonstration that the catalytic reactivity of RuNPs is as high as that of PtNPs in photocatalytic hydrogen evolution. Ruthenium-based materials have to date been utilized mainly for electrocatalytic hydrogen evolution.[32−35] In the present photocatalytic system, 2-phenyl-4-(1-naphthyl)-quinolinium perchlorate ($QuPh^+$—NA) and dihydronicotinamide adenine dinucleotide (NADH) are used as the donor—acceptor photocatalyst and electron donor, respectively (Scheme 1). Nanosecond laser flash photolysis and kinetic measurements revealed that $QuPh^•$—NA, the quinolinyl radical produced by the photoirradiation of $QuPh^+$—NA with NADH, injects an electron to RuNPs and PtNPs to evolve hydrogen. The effects of pH and the size of the RuNPs on both the catalytic reactivity for hydrogen evolution and the electron injection from $QuPh^•$—NA were also examined in detail to optimize the catalytic reactivity.

EXPERIMENTAL SECTION

Materials. Triruthenium dodecacarbonyl [$Ru_3(CO)_{12}$], stearylamine (>80%), tri-*n*-octylamine, 1-octadecene (ODE, 90%), and poly(vinylpyrrolidone) (PVP, M_w = 40 000) were obtained from Tokyo Chemical Industry Co., Ltd. Ruthenium(III) chloride ($RuCl_3 \cdot nH_2O$, 38% Ru) and Pt—PVP nanoparticles (2 nm) were supplied by Tanaka Kikinzoku Kogyo. Oleylamine (70%) was purchased from Sigma-Aldrich. 2-Phenyl-4-(1-naphtyl)quinolinium perchlorate was synthesized by the reported method.[13a] Each buffer solution were prepared by addition of NaOH to an aqueous solution containing 50 mM of electrolyte (phthalate for pH 4.5, phosphate for pH 7.0, 8.0 or 12, or potassium chloride for pH 13) or 25 mM of carbonate for pH 10 or 11. All chemicals were used without further purification unless otherwise noted.

Synthesis of Size-Controlled RuNPs. Size-controlled RuNPs were synthesized by thermal decomposition of Ru complexes in an organic solvent according to literature procedures[36] as described below.

Synthesis of 2.0 nm RuNPs.[36a] $RuCl_3 \cdot nH_2O$ (0.065 mmol) was dissolved in 4 mL of oleylamine in a 50 mL three-neck round-bottom flask at room temperature. The solution was degassed under reduced pressure for 20 min at 373 K and then heated to 543 K (at 2.2 K min^{-1}) and kept at this temperature for 20 min under an Ar atmosphere. After the solution was cooled to room temperature, 4 mL of toluene was added. Ethanol was then added to cause flocculation, and the mixture was centrifuged (15 000 rpm, 10 min) to separate the black precipitates, which were further purified by three repeated dispersion/precipitation (toluene/ethanol) cycles. The final product was dispersed in 5 mL of *n*-hexane.

Synthesis of 3.3 nm RuNPs.[36b] $Ru_3(CO)_{12}$ (0.047 mmol) and stearylamine (3.7 mmol) were dissolved in 4 mL of tri-*n*-octylamine in a 50 mL three-neck round-bottom flask at room temperature. The solution was degassed under reduced pressure for 20 min at 373 K and then heated to 543 K (at 3.1 K min^{-1}) and kept at this temperature for 20 min under an Ar atmosphere. After the solution was cooled to room temperature, 4 mL of toluene was added, and the solution was centrifuged (4000 rpm, 10 min) to separate a trace amount of solids. Ethanol was then added, and the suspension was centrifuged (15 000 rpm, 10 min) to separate the black precipitates, which were washed three times by dispersion/precipitation cycles. The final product was dispersed in 5 mL of *n*-hexane.

Synthesis of 6.5 nm RuNPs.[36b] $Ru_3(CO)_{12}$ (0.047 mmol) was dissolved in 4 mL of oleylamine in a 50 mL three-neck round-bottom flask at room temperature. The mixed solution was degassed under reduced pressure for 20 min at room temperature and then heated to 543 K (at 3.5 K min^{-1}) and kept at this temperature for 20 min under an Ar atmosphere. After the solution was cooled to room temperature, 4 mL of toluene was added. Ethanol was then added, and the suspension was centrifuged (15 000 rpm, 10 min) to separate the black precipitates, which were washed three times by dispersion/precipitation cycles. The final product was dispersed in 5 mL of *n*-hexane.

Synthesis of 4.1 and 8.0 nm RuNPs.[36b] $Ru_3(CO)_{12}$ (0.047 mmol for 4.1 nm or 0.094 mmol for 8.0 nm) was dissolved in 4 mL of tri-*n*-octylamine in a 50 mL three-neck round-bottom flask at room temperature. The solution was degassed under reduced pressure for 20 min at 373 K and then heated to 543 K (at 3.1 K min^{-1} for 4.1 nm or 2.3 K min^{-1} for 8.0 nm) and kept at this temperature for 20 min under an Ar atmosphere. After the solution was cooled to room temperature, 4 mL of toluene was added to cause flocculation. Ethanol was then added, and the suspension was centrifuged (15 000 rpm, 10 min) to separate the black precipitates, which were washed three times by dispersion/precipitation cycles. The final product was dispersed in 5 mL of *n*-hexane.

Synthesis of FeNPs.[37] ODE (20 mL) and oleylamine (0.3 mL) were mixed and degassed by passing Ar gas (99.999% purity) through the mixture at 393 K for 30 min. The temperature was raised to 453 K (at 3.3 K min^{-1}), and $Fe(CO)_5$ (0.7 mL, 5.2 mmol) was slowly added. The mixture was kept at the temperature for 20 min. After the solution was cooled to room temperature, ethanol was added to cause flocculation, and then the suspension was centrifuged (15 000 rpm, 10 min) to separate the black precipitates, which were washed three times by dispersion/precipitation cycles. The final product was dispersed in 5 mL of *n*-hexane.

Surfactant Exchange with PVP. An *n*-hexane solution (2.5 mL) containing nanoparticles stabilized by oleylamine or tri-*n*-octylamine was mixed with a solution containing PVP (200 mg, M_w = 40 000) in $CHCl_3$ (2 mL) at room temperature. The solution was stirred for 24 h to exchange the surfactant. A certain amount of acetone was added to the solution to cause flocculation, and then the mixture was centrifuged at 15 000 rpm for 10 min. The collected water-soluble particles were washed three times by dispersion/precipitation (water/acetone) cycles.

Transmission Electron Microscopy. The sizes of nanoparticles were determined from bright-field transmission electron microscopy (TEM) images obtained using a JEOL JEM-2100 transmission electron microscope equipped with a cold field-emission gun with an accelerating voltage of 200 keV. The observed samples were prepared by dropping a solution of nanoparticles and allowing the solvent to evaporate, after which the nanoparticles were scooped up with an amorphous carbon supporting film.

Photocatalytic Hydrogen Evolution. A mixed solution (2.0 mL) of an aqueous buffer (pH 4.5, 7.0, 8.0, 10, 11, 12, or 13) and MeCN [1:1 (v/v)] containing $QuPh^+$—NA (0.22 mM), NADH (1.0 mM), and RuNPs (25 μg) was flushed with N_2 gas. The solution was then irradiated with a Xe lamp (Ushio Optical, Model X SX-UID 500X AMQ) through a color filter glass (Toshiba Glass UV-35) transmitting $\lambda > 340$ nm at room

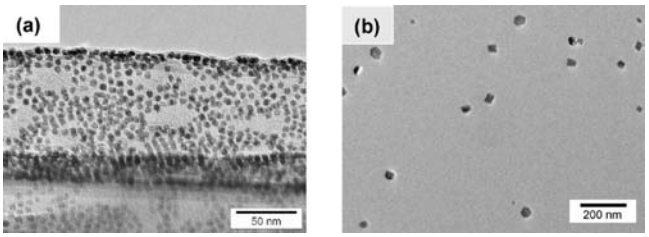

Figure 1. TEM images of (a) 4.1 nm RuNPs and (b) FeNPs.

temperature. After the solution was stirred for 1 min in the dark, the gas in the headspace was analyzed using a Shimadzu GC-14B gas chromatograph (detector, TCD; column temperature, 50 °C; column, active carbon with 60−80 mesh particle size; carrier gas, N_2) to quantify the evolved hydrogen.

Kinetic Measurements. Typically, a mixed solution (2.0 mL) of a deaerated aqueous buffer (pH 4.5, 7.0, 8.0, 10, or 11) and MeCN [1:1 (v/v)] containing $QuPh^+$−NA (0.44 mM) and NADH (1.0 mM) was photoirradiated for 1 min with a Xe lamp through a color filter glass transmitting $\lambda > 340$ nm. Next, a deaerated aqueous solution containing RuNPs or PtNPs (3.0 μg) was added to the photoirradiated solution using a microsyringe with stirring. Rate constants of electron transfer from $QuPh^{\bullet}$−NA (obtained by one-electron reduction of $QuPh^+$−NA) to the catalyst were determined from the decay of absorption at 420 nm due to $QuPh^{\bullet}$−NA, which was monitored using a Hewlett-Packard 8453 diode-array spectrophotometer with a quartz cuvette (path length 10 mm) at 298 K.

■ RESULTS AND DISCUSSION

Photocatalytic Hydrogen Evolution with Ru and Fe Nanoparticles. RuNPs and FeNPs used as hydrogen-evolution catalysts were prepared by thermal decomposition of $Ru_3(CO)_{12}$ and $Fe(CO)_5$, respectively, in the presence of tri-*n*-octylamine for RuNPs and oleylamine for FeNPs as the capping agent in an organic solvent following literature procedures (see the Experimental Section).[36,37] The obtained nanoparticles were characterized by TEM, as displayed in Figure 1. The RuNPs had a spherical shape, whereas the FeNPs were spherical (~60%) or cuboidal particles (~40%). The diameters of the RuNPs and FeNPs were determined to be 4.1 ± 0.6 and 12 ± 5 nm, respectively. The capping agents of these nanoparticles were exchanged to PVP before the photocatalytic hydrogen-evolution measurements in order to increase the dispersity in aqueous solution.

Figure 2 shows the time course of hydrogen evolution in the reaction system composed of NADH, $QuPh^+$−NA, and metal nanoparticles (MNPs, M = Ru, Fe, Pt) as the sacrificial electron donor, photocatalyst, and hydrogen-evolution catalyst, respectively. No hydrogen evolution was observed from a mixed solution (2.0 mL) of a deaerated phthalate buffer (pH 4.5) and MeCN [1:1 (v/v)] containing $QuPh^+$−NA (0.22 mM), NADH (1.0 mM), and MNPs (12.5 mg L^{-1}) in the dark. Photoirradiation ($\lambda > 340$ nm) of the solution resulted in efficient hydrogen evolution. The amount of evolved hydrogen was determined by gas chromatography after 1 min of stirring in the dark (see the Experimental Section). The volume of evolved hydrogen would be 2.0 μmol if NADH, the sacrificial electron donor, were completely consumed for hydrogen evolution. When 2 nm PtNPs were used as the hydrogen-evolution catalyst (Figure 2, red), highly efficient hydrogen evolution was observed in which the stoichiometric amount of hydrogen was evolved within 4

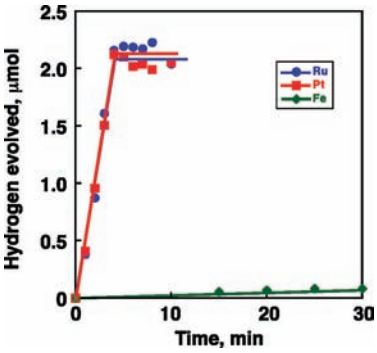

Figure 2. Time course of hydrogen evolution under photoirradiation ($\lambda > 340$ nm) of a deaerated mixed solution of a phthalate buffer (pH 4.5) and MeCN [1:1 (v/v)] containing $QuPh^+$−NA (0.22 mM), NADH (1.0 mM), and various catalysts [12.5 mg L^{-1}; (blue) 4.1 nm RuNPs, (red) 2 nm PtNPs, (green) 10 nm FeNPs] at 298 K.

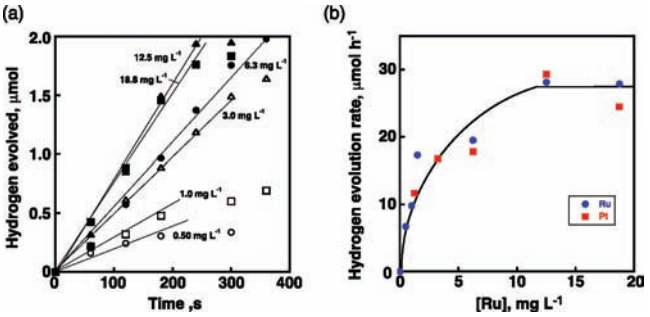

Figure 3. (a) Time courses of hydrogen evolution under photoirradiation ($\lambda > 340$ nm) of deaerated mixed solutions (2.0 mL) of a phthalate buffer (pH 4.5) and MeCN [1:1 (v/v)] containing $QuPh^+$−NA (0.22 mM), NADH (1.0 mM), and various loadings of RuNPs [○, 0.50 mg L^{-1}; □, 1.0 mg L^{-1}; △, 1.5 mg L^{-1}; ○, 6.3 mg L^{-1}; ■, 12.5 mg L^{-1}; ▲, 18.8 mg L^{-1}] at 298 K. (b) Plots of the hydrogen-evolution rate vs concentration for RuNPs (blue) and PtNPs (red). The hydrogen-evolution rates were determined from the initial (<120 s) slopes of the time courses of hydrogen evolution.

min. It is important to emphasize that virtually the same hydrogen-evolution rate was observed when the PtNPs were replaced by 4.1 nm RuNPs (Figure 2, blue). When FeNPs were used as the hydrogen-evolution catalyst, however, only a small amount of hydrogen was evolved (Figure 2, green). No stoichiometric amount of hydrogen was evolved with FeNPs even after 30 min. The slow hydrogen evolution with FeNPs is due to slow electron transfer from the photogenerated radical species to FeNPs [see Figure S1 in the Supporting Information (SI)]. Thus, we focused on examining the dependence of the catalytic reactivity of the RuNPs on pH and also on the particle size, including kinetic measurements.

Photocatalytic Hydrogen Evolution with RuNPs under Various Conditions. Time courses of hydrogen evolution for various weight concentrations of RuNPs in the reaction solution are shown in Figure 3a. The hydrogen-evolution rate increased in proportion to the concentration of RuNPs up to 12.5 mg L^{-1} (blue), reaching the value of 28 μmol h^{-1}, as shown in Figure 3b. Even when the concentration of RuNPs was further increased to 18.8 mg L^{-1}, the hydrogen-evolution rate remained at 28 μmol h^{-1}. Photocatalytic hydrogen evolution was also carried out with PtNPs at concentrations of 1.3, 3.3, 6.3, and 12.5 mg L^{-1} as the

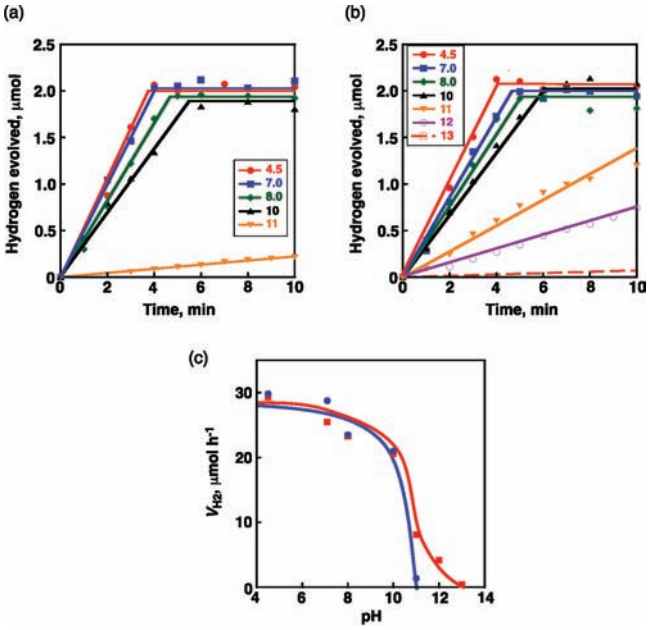

Figure 4. Time courses of evolved hydrogen under photoirradiation (λ > 340 nm) of deaerated mixed solutions (2 mL) of aqueous buffers with various pH values and MeCN [1:1 (v/v)] containing $QuPh^+$−NA (0.22 mM), NADH (1.0 mM) with (a) RuNPs (12.5 mg L^{-1}) or (b) PtNPs (12.5 mg L^{-1}) at 298 K. (c) The pH dependences of hydrogen-evolution rates (V_{H2}) of MNPs [*M* = Pt (red, 12.5 mg) and Ru (blue, 12.5 mg)].

hydrogen-evolution catalyst (Figure 3b, red). The hydrogen-evolution rates achieved using PtNPs with different concentrations were comparable to the rates obtained with the same concentrations of RuNPs. These results indicate that the catalytic reactivity of RuNPs for photocatalytic hydrogen evolution is really comparable to that of PtNPs.

A repetitive test with the RuNPs for the photocatalytic hydrogen evolution was carried out under the same conditions as described above. At the end of each reaction, NADH was added to the reaction solution, and the solution was photoirradiated to determine the amount of evolved hydrogen. As indicated in Figure S2 in the SI, the hydrogen evolution in the second cycle was as fast as that in the first cycle, although the hydrogen evolution became slightly slower at the third cycle.

With this catalytic reaction system using RuNPs as the hydrogen-evolution catalyst, visible light (λ > 400 nm) could also be used for hydrogen evolution, although the hydrogen-evolution rate (8.3 μmol h^{-1}; red data in Figure S3b in the SI) was lower than the rate for UVA (λ > 340 nm) irradiation (28 μmol h^{-1}; blue data in Figure S3b in the SI) because of the small absorption coefficient of $QuPh^+$-NA in the visible region (Figure S3a in the SI).

Photocatalytic Hydrogen Evolution with RuNPs and PtNPs under Various pH Conditions. The photocatalytic hydrogen-evolution experiments were performed with a mixture of an aqueous buffer and MeCN [1:1 (v/v)] containing $QuPh^+$−NA (0.22 mM), NADH (1.0 mM), and RuNPs (12.5 mg L^{-1}) under various pH conditions. Figure 4a shows the amount of evolved hydrogen as a function of photoirradiation time at pH 4.5, 7.0, 8.0, 10, and 11. Nearly stoichiometric amounts of hydrogen were evolved at pH 4.5−10. The hydrogen-evolution rates decreased with increasing pH of the solution. At pH 11, no stoichiometric amount of hydrogen was evolved even after 10 min (Figure 4a, orange). The catalytic reactivity of PtNPs for photocatalytic hydrogen evolution was also examined under various pH conditions. Figure 4b shows the time course of hydrogen evolution using PtNPs as the hydrogen-evolution catalyst under the same reaction conditions as the case of RuNPs. The stoichiometric amount of hydrogen was evolved at pH 4.5−10. The hydrogen-evolution rate decreased with increasing pH. At pH 11, the amount of evolved hydrogen was less than the stoichiometric amount after photoirradiation for 10 min. It is interesting to note that a small amount of hydrogen evolution was still observed at pH 12.

The catalytic reactivities of RuNPs and PtNPs were compared in terms of the hydrogen-evolution rates determined from the initial slopes in Figure 4a,b. The specific hydrogen-evolution rates were normalized by the weight concentrations of MNPs for comparison between RuNPs and PtNPs. The hydrogen-evolution rates (V_{H_2}) are plotted against pH in Figure 4c [RuNPs (blue) and PtNPs (red)]. In all pH regions, the specific hydrogen-evolution rates obtained with RuNPs were comparable to those obtained with PtNPs in the pH region below 10. The sudden reactivity loss around pH 11 observed for both RuNPs and PtNPs indicates that the rate-determining step in this pH region is highly influenced by the proton concentration. It should be emphasized that the significant hydrogen-evolution rate was maintained up to pH 10. To the best of our knowledge, this is the first example of photocatalytic hydrogen evolution with RuNPs under basic conditions around pH 10.

Photocatalytic hydrogen evolution under basic conditions has been reported for several reaction systems with both homogeneous and heterogeneous catalysts.[16b,38,39] Among homogeneous catalysts, $[Co(dmgBF_2)_2(OH_2)_2]$ [**1**; $dmgBF_2$ = (difluoroboryl)-dimethylglyoximate anion] exhibits the highest reactivity under basic conditions.[15,16b,39a] For example, photoirradiation (λ > 400 nm) of a mixed solution of H_2O and MeCN containing triethylamine, rose bengal (0.40 mM), and catalyst **1** (0.40 mM) generated hydrogen for 5 h with a turnover frequency of 230 h^{-1} and a turnover number of 327 under pH 10 conditions.[39a] On the other hand, the results for the photocatalytic hydrogen-evolution system with 4.1 nm RuNPs operated under pH 10 conditions indicated that the turnover frequency and turnover number normalized by the number of surface Ru atoms were as high as ∼1050 h^{-1} and ∼300, respectively[40] (see page S8 in the SI for calculation procedures). For the reaction system with heterogeneous catalysts, hydrogen evolution was observed by photoirradiation of an aqueous solution containing rose bengal as a photosensitizer and triethylamine as a sacrificial electron donor with colloidal Pt under basic conditions.[10a] The optimal pH condition for this system was pH 8, with a hydrogen-evolution rate of 56.9 μmol h^{-1} from 60 mL of solution (0.95 μmol h^{-1} mL^{-1}) with 7.5 mg L^{-1} colloidal Pt.[10a] Additionally, the hydrogen-evolution system composed of *N*-tetradecyl-*N*′-methyl-4,4′-dipyridinium dichloride ($C_{14}MV^{2+}$) and Pt/TiO_2 as a catalyst under pH 12 conditions has been reported.[10b] Photoirradiation of an aqueous solution (5 mL) containing MV^+, polyvinyl alcohol, and 1.5% Pt/TiO_2 (500 mg L^{-1}) produced hydrogen at a rate of 22 μmol h^{-1} from 5 mL of solution (4.5 μmol h^{-1} mL^{-1}).[10b] The photocatalytic system with RuNPs as the hydrogen-evolution catalyst exhibited the high hydrogen-evolution rate of 28 μmol h^{-1} from 2 mL of solution (14 μmol h^{-1} mL^{-1}) with 12.5 mg L^{-1} RuNPs under pH 10 conditions.

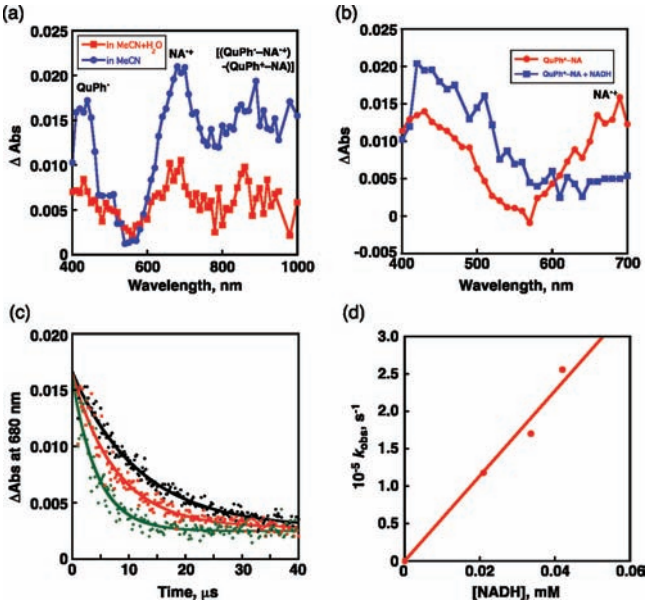

Figure 5. (a) Transient absorption spectra of $QuPh^+$—NA (0.052 mM) in MeCN (blue ●) and in a mixed solution of deaerated aqueous buffer (pH 4.5) and MeCN [1:1 (v/v)] (red ■) at 298 K taken 4 μs after nanosecond laser excitation at 355 nm. (b) Transient absorption spectra of $QuPh^+$—NA (0.052 mM) with (blue ■) and without (red ●) NADH (0.084 mM) in a mixed solution (2.0 mL) of deaerated aqueous buffer (pH 4.5) and MeCN [1:1 (v/v)] 2.4 μs after nanosecond laser excitation. (c) Decay time profiles of the absorption at 680 nm due to $QuPh^{\bullet}$—$NA^{\bullet+}$ at various concentrations of NADH (green, 0.042 mM; red, 0.034 mM; black, 0.021 mM) in the presence of $QuPh^+$—NA (0.026 mM). (d) Plot of the pseudo-first-order rate constant (k_{obs}) for electron transfer from NADH to $QuPh^{\bullet}$—$NA^{\bullet+}$ vs [NADH].

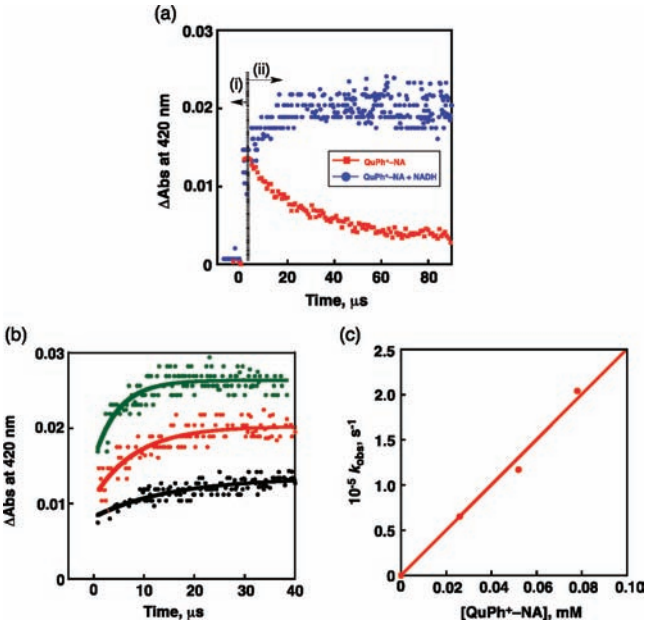

Figure 6. (a) Time profiles of the formation and decay of the absorption at 420 nm due to $QuPh^{\bullet}$—NA as detected by nanosecond laser excitation at 355 nm of a mixed solution of a deaerated phthalate buffer (pH 4.5) and MeCN [1:1 (v/v)] containing $QuPh^+$—NA (0.052 mM) at 298 K in the absence (red ■) and presence (blue ●) of NADH (0.084 mM). (b) Time profiles of the absorption at 420 nm due to $QuPh^{\bullet}$—NA for various concentrations of $QuPh^+$—NA (green, 0.078 mM; red, 0.052 mM; black, 0.026 mM) in the presence of NADH (0.084 mM). (c) Plot of the pseudo-first-order rate constant (k_{obs}) for electron transfer from $NAD^{\bullet}$ to $QuPh^+$—NA vs [$QuPh^+$—NA].

Formation of $QuPh^{\bullet}$—NA by Photoinduced Reduction of $QuPh^+$—NA with NADH. Nanosecond laser flash photolysis measurements of $QuPh^+$—NA were conducted to detect the electron-transfer state ($QuPh^{\bullet}$—$NA^{\bullet+}$) in the absence and presence of NADH. Laser excitation at 355 nm of a mixed solution of a deaerated aqueous buffer and MeCN [1:1 (v/v)] containing $QuPh^+$—NA (0.052 mM) resulted in formation of the electron-transfer state ($QuPh^{\bullet}$—$NA^{\bullet+}$) with a quantum yield of 0.34, as determined by comparison with a transient absorption band at 420 nm due to $QuPh^{\bullet}$—$NA^{\bullet+}$ in MeCN (0.83)[13a] (Figure 5a, red; Figure S4 in the SI). Formation of $QuPh^{\bullet}$—$NA^{\bullet+}$ in MeCN was more clearly seen by the transient absorptions at λ_{max} = 420 nm ($QuPh^{\bullet}$ moiety) and 680 nm ($NA^{\bullet+}$ moiety) (Figure 5a, blue). Additionally, the broad band appearing at λ > 800 nm evidenced the formation of the π-dimer radical cation, [($QuPh^{\bullet}$—$NA^{\bullet+}$)-($QuPh^+$—NA)] in both MeCN and a mixed solution of an aqueous buffer and MeCN, because there was no transient absorption band in the near-IR region due to the π-dimer radical cation in the case of femtosecond laser flash photolysis measurements.[13a,41] The transient absorption at 680 nm due to [($QuPh^{\bullet}$— $NA^{\bullet+}$)-($QuPh^+$—NA)] disappeared in the presence of 0.084 mM NADH (Figure 5b, blue) because electron transfer from NADH to the $NA^{\bullet+}$ moiety of the π-dimer radical cation occurs, as predicted by the higher one-electron reduction potential of the $NA^{\bullet+}$ moiety (E_{red} = 1.87 V vs SCE)[13a] in comparison with the one-electron oxidation potential of NADH (E_{ox} = 0.76 V vs SCE).[29,42]

The rate of electron transfer from NADH to the $NA^{\bullet+}$ moiety of the π-dimer radical cation was monitored by the decay of the absorption at 680 nm for various concentrations of NADH (green, 0.042 mM; red, 0.034 mM; black, 0.021 mM), as shown in Figure 5c. The rate obeyed pseudo-first-order kinetics, and the pseudo-first-order rate constant (k_{obs}) increased linearly with increasing concentration of NADH, as shown in Figure 5d. The second-order rate constant (k_{ox}) of electron transfer from NADH to the $NA^{\bullet+}$ moiety of the π-dimer radical cation was determined from the slope of the linear plot in Figure 5d to be 5.7 × 10^9 M^{-1} s^{-1}, which is close to the diffusion-limited value.[13c,29,43]

In contrast to the decay of the absorption at 680 nm due to the $NA^{\bullet+}$ moiety of the π-dimer radical cation by the electron-transfer reduction with NADH, a rise in absorption at 420 nm due to the $QuPh^{\bullet}$ moiety was observed in the presence of NADH, as shown in Figure 6a. In the absence of NADH, the absorption at 420 nm due to the π-dimer radical cation decayed because of the bimolecular back electron transfer to the ground state (Figure 6a, red).[13a,41] In the presence of NADH, however, the absorption at 420 nm due to the $QuPh^{\bullet}$ moiety increased rather than decreased following the rapid formation of the π-dimer radical cation (Figure 6a, blue). The rate of additional formation of the $QuPh^{\bullet}$ moiety obeyed pseudo-first-order kinetics, and the pseudo-first-order rate constant (k_{obs}) increased linearly with increasing concentration of $QuPh^+$—NA. This indicates that $QuPh^{\bullet}$—NA is formed by the electron-transfer reduction of $QuPh^+$—NA by $NAD^{\bullet}$, which is formed by deprotonation of $NADH^{\bullet+}$ following electron transfer from NADH to the $NA^{\bullet+}$ moiety of the π-dimer radical cation.[41,44] The electron transfer from $NAD^{\bullet}$ to $QuPh^+$—NA is thermodynamically feasible, because the one-electron oxidation potential of $NAD^{\bullet}$

Scheme 2. Photoinduced Electron Transfer from NADH to $QuPh^+-NA$

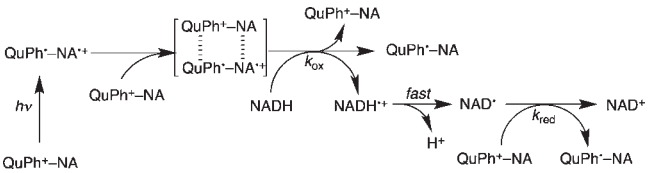

(E_{ox} = −1.1 V vs SCE)[42a] is more negative than the one-electron reduction potential of the $QuPh^+$ moiety in $QuPh^+-NA$ (E_{red} = −0.90 V vs SCE).[13a,45,46] The second-order rate constant (k_{red}) of the electron-transfer reduction of $QuPh^+-NA$ by $NAD^•$ was determined from the slope of the linear plot in Figure 6c to be 2.5×10^9 M^{-1} s^{-1}.

The overall reaction pathway for formation of $QuPh^•-NA$ is shown in Scheme 2. Upon photoexcitation of $QuPh^+-NA$, the electron-transfer state of $QuPh^+-NA$ ($QuPh^•-NA^{•+}$) is produced, followed by formation of the π-dimer radical cation with $QuPh^+-NA$, $[(QuPh^•-NA^{•+})(QuPh^+-NA)]$. Electron transfer from NADH to the $NA^{•+}$ moiety of the π-dimer radical cation occurs, producing $NADH^{•+}$, $QuPh^•-NA$, and $QuPh^+-NA$. $NADH^{•+}$ undergoes facile deprotonation to produce $NAD^•$,[41,44] from which an electron is transferred to $QuPh^+-NA$ to produce an additional $QuPh^•-NA$ and NAD^+. Thus, 2 equiv of $QuPh^•-NA$ are formed through the photoinduced reduction of $QuPh^+-NA$ by NADH.

Electron Transfer from $QuPh^•-NA$ to MNPs (M = Ru, Pt). Rates of electron transfer from $QuPh^•-NA$ to MNPs (M = Ru, Pt) in a mixed solution of phthalate buffer (pH 4.5) and MeCN [1:1 (v/v)] were determined by UV−vis spectral changes for comparison with the corresponding rates of hydrogen evolution determined by gas chromatography. This is the first example to observe the electron-transfer rate from a radical species to RuNPs and compare it with the hydrogen-evolution rate. An aliquot (2.0 mL) of $QuPh^+-NA$ (0.44 mM) was photoirradiated in the presence of NADH (1.0 mM) for several minutes to generate $QuPh^•-NA$. Next, a small portion of an aqueous solution containing MNPs (3.0 μg, 1.5 mg L^{-1}) was added to the mixed solution containing $QuPh^•-NA$ to initiate the hydrogen evolution. Figure 7 depicts the time profiles of the UV−vis absorption change at 420 nm (blue ●) and those of the amount of evolved hydrogen quantified by gas chromatography (red ●) for RuNPs and PtNPs. In both cases, the total amount of evolved hydrogen was 0.42 μmol, which corresponds to more than 80% of the stoichiometric amount of hydrogen predicted from the absorption change due to $QuPh^•-NA$. As shown in Figure 7, the decays of $QuPh^•-NA$ due to electron transfer from $QuPh^•-NA$ to MNPs were complete within 30 s (blue lines), whereas the hydrogen evolution lasted for a longer period (~400 s). This indicates that the hydrogen evolution occurs after the electron transfer from $QuPh^•-NA$ to the MNPs.

The rates of electron transfer from $QuPh^•-NA$ to MNPs (M = Ru, Pt) obeyed first-order kinetics, and the first-order rate constants increased linearly with increasing MNP weight concentration at various pH. The electron-transfer rate constants (k_{et}) were determined from the slopes of the linear plots of k_{obs} versus MNP weight concentration in Figure 8a,b for RuNPs and PtNPs, respectively. The k_{et} values for RuNPs were similar to those for PtNPs, and in both cases, the k_{et} values were rather invariant with respect to pH (Figure 8c). Such a small dependence

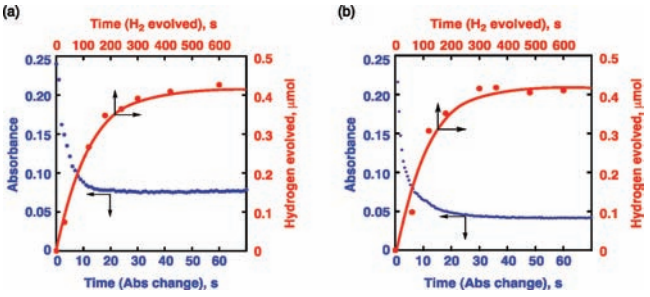

Figure 7. Decay time profiles of absorption at 420 nm due to $QuPh^•-NA$ in electron transfer from $QuPh^•-NA$ to (a) RuNPs (1.5 mg L^{-1}) or (b) PtNPs (1.5 mg L^{-1}) (blue) and corresponding time profiles of hydrogen evolution (red) in mixed solutions of a phthalate buffer (pH 4.5) and MeCN [1:1 (v/v)]. $QuPh^•-NA$ was produced by photoirradiation of $QuPh^+-NA$ (0.44 mM) in the presence of NADH (1.0 mM).

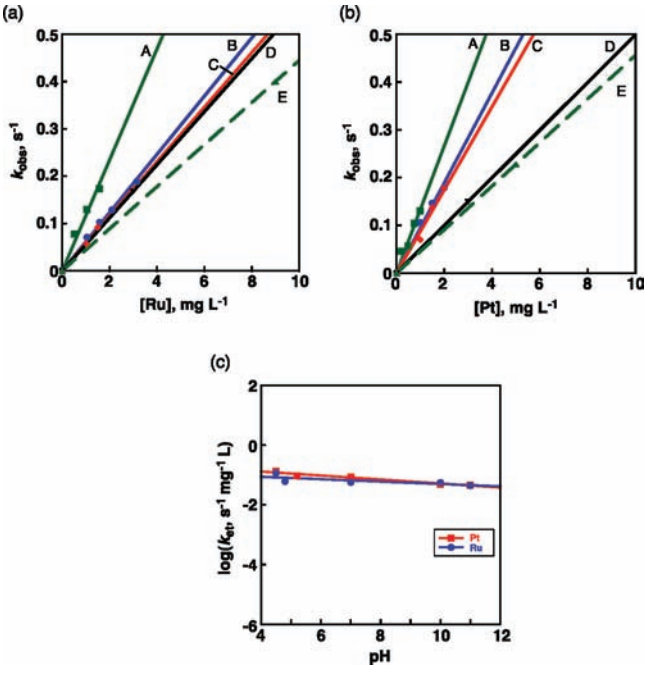

Figure 8. Plots of the pseudo-first-order rate constants (k_{obs}) for electron transfer from $QuPh^•-NA$ vs weight concentrations of (a) RuNPs and (b) PtNPs on the surface [A (green), pH 4.5; B (blue), pH 4.8 (Ru) or 5.2 (Pt); C (red), pH 7.0; D (black), pH 10; E (dashed green), pH 11]. (c) pH dependence of the rate constants (k_{et}) for electron transfer from $QuPh^•-NA$ to PtNPs (red) and RuNPs (blue) determined from slopes of the plots in (a) and (b).

of k_{et} on pH shows a sharp contrast to the case of photocatalytic hydrogen evolution with 9-mesityl-10-methylacridinium ion (Acr^+-Mes), in which the rate of electron transfer from the acridinyl radical ($Acr^•-Mes$) to PtNPs agreed with the rate of hydrogen evolution and the electron-transfer rate increased with decreasing pH.[29]

The important difference between Acr^+-Mes and $QuPh^+-NA$ is the one-electron reduction potentials of the electron-acceptor moieties. The one-electron reduction potential of $QuPh^+-NA$ (E_{red} = −0.90 V vs SCE),[13a,45,46] which is equivalent to the one-electron oxidation potential of $QuPh^•-NA$, is significantly more

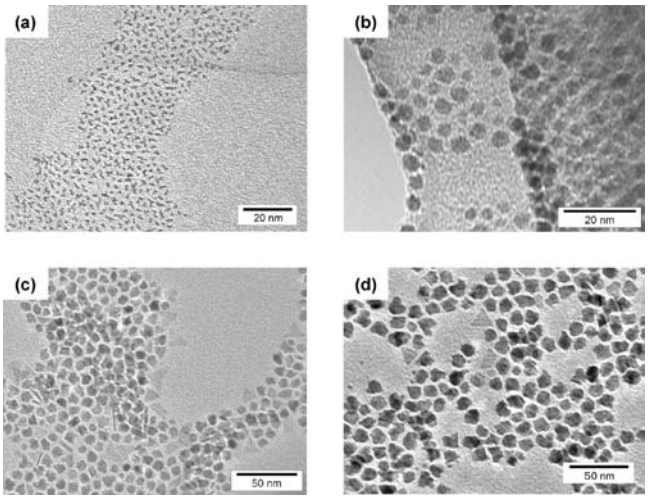

Figure 9. TEM images of RuNPs with sizes of (a) 2.0, (b) 3.3, (c) 6.5, and (d) 8.0 nm.

negative than that of Acr^+—Mes (E_{red} = −0.57 V vs SCE).[13a,47] In the case of Acr^+—Mes, electron transfer from $Acr^•$—Mes to PtNPs requires the assistance of a proton, and the rate of the proton-coupled electron transfer increases with increasing proton concentration. In contrast to this, electron transfer from $QuPh^•$—NA to MNPs occurs without assistance of a proton because of the much stronger reducing ability of $QuPh^•$—NA in comparison with $Acr^•$—Mes, as indicated by the significantly more negative oxidation potential of $QuPh^•$—NA (E_{ox} = −0.90 V vs SCE)[13a] than that of $Acr^•$—Mes (E_{ox} = −0.57 V vs SCE).[13a,47]

Thus, the rate of electron transfer from $QuPh^•$—NA to MNPs remains rather constant even under highly basic conditions (pH > 10). Because the rate of hydrogen evolution was much lower than the rate of electron transfer from $QuPh^•$—NA to MNPs, multielectron reduction of MNPs may be required to evolve hydrogen. The reaction of multielectron-reduced MNPs with protons to evolve hydrogen is not the rate-determining step at pH < 10, as indicated by the pH dependence of the hydrogen evolution (Figure 4c). At pH > 11, however, the rate of hydrogen evolution decreases with increasing pH.

Effect of the Size of the RuNPs on the Photocatalytic Hydrogen Evolution. TEM images of RuNPs with different sizes are displayed in Figure 9. The size-controlled RuNPs were prepared by thermal decomposition of $Ru_3(CO)_{12}$ or $RuCl_3$ in an organic solvent (stearylamine, tri-*n*-octylamine, 1-octadecene, or oleylamine) at high temperature (see the Experimental Section). The RuNPs smaller than 4.1 nm had no specific shape, whereas samples of RuNPs with sizes of 6.5 and 8.0 nm contained triangular platelets. Further characterizations of the RuNPs by powder X-ray diffraction and dynamic laser scattering are shown in Figures S5 and S6 in the SI.

The photocatalytic hydrogen evolution was conducted under photoirradiation of a mixed solution (2.0 mL) of deaerated buffer (pH 4.5) and MeCN [1:1 (v/v)] containing $QuPh^+$—NA (0.22 mM), NADH (1.0 mM), and RuNPs (12.5 mg L^{-1}) with different sizes (2—8 nm). When RuNPs with sizes of 3.3—8.0 nm were employed as hydrogen-evolution catalysts, nearly stoichiometric amounts of hydrogen were evolved (B—E in Figure 10a), but the amount of evolved hydrogen was ~80% of the stoichiometric amount in the case of 2.0 nm RuNPs (A in Figure 10a). The hydrogen-evolution rates (V_{H_2}) normalized by the weight

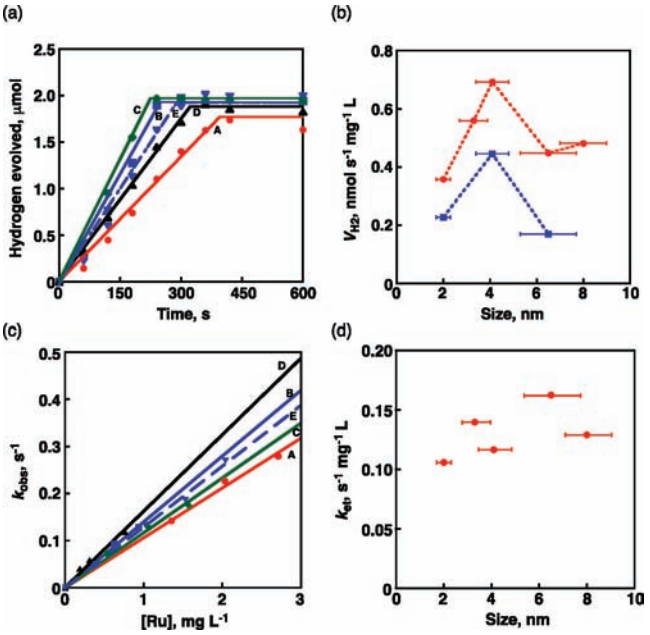

Figure 10. (a) Time courses of hydrogen evolution under photoirradiation (λ > 340 nm) of mixed solutions of deaerated phthalate buffer (pH 4.5) and MeCN [1:1 (v/v)] containing NADH (1.0 mM), $QuPh^+$—NA (2.2 mM), and RuNPs with different sizes [12.5 mg L^{-1}; (A) 2.0 nm, (B) 3.3 nm, (C) 4.1 nm, (D) 6.5 nm, (E) 8.0 nm]. (b) Plots of hydrogen-evolution rates at different RuNP concentrations (red, 12.5 mg L^{-1}; blue, 6.3 mg L^{-1}) vs the size of RuNPs. (c) Plots of the pseudo-first-order rate constants (k_{obs}) for electron transfer from $QuPh^•$—NA vs weight concentrations of RuNPs [(A) 2.0 nm; (B) 3.3 nm; (C) 4.1 nm; (D) 6.5 nm; (E) 8.0 nm]. (d) Size dependence of the rate constants (k_{et}) for electron transfer from $QuPh^•$—NA to RuNPs with various sizes, as determined from the slopes of the plots in (c).

concentration of RuNPs (12.5 mg L^{-1}) are plotted against the size of the RuNPs in Figure 10b (red). The 4.1 nm RuNPs showed the highest reactivity per unit catalyst weight. The highest hydrogen-evolution rate was also observed for the 4.1 nm RuNPs under conditions using a reduced concentration of RuNPs (6.3 mg L^{-1}; Figure 10b, blue, and Figure S7 in the SI). The rate constants for electron transfer from $QuPh^•$—NA to RuNPs with different sizes were determined from the slopes of the linear plots of k_{obs} versus the weight concentration of RuNPs (Figure 10c), where k_{obs} is the pseudo-first-order rate constant determined from the first-order plots. A mixed solution (2.0 mL) of phthalate buffer and MeCN [1:1 (v/v)] containing $QuPh^+$—NA (0.44 mM) was photoirradiated in the presence of NADH (1.0 mM) to generate $QuPh^•$—NA until no significant absorption change was observed. Next, a small portion of an aqueous solution containing RuNPs (3.0 μg, 1.5 mg L^{-1}) was added to the solution containing $QuPh^•$—NA to initiate the electron transfer to RuNPs. There was no apparent effect of size on the electron-injection rate constant normalized by the weight concentration, as shown in Figure 10d. This seems to be reasonable because injected electrons may be delocalized over the whole body of the RuNPs.

Such size-dependent catalysis by RuNPs has been reported for catalytic CO oxidation by O_2 using RuNPs with sizes of 2—6 nm.[48] The CO oxidation reactivity increased with the size, and 6 nm RuNPs showed 8-fold higher reactivity than 2 nm RuNPs. Similarly, size-dependent catalysis by RuNPs has been reported for the catalytic hydrogenation of 1,3-cyclohexadiene

Scheme 3. Size Effects of RuNPs on the Reaction Rates for the "Proton Reduction" and "Hydrogen-Atom Association" Steps

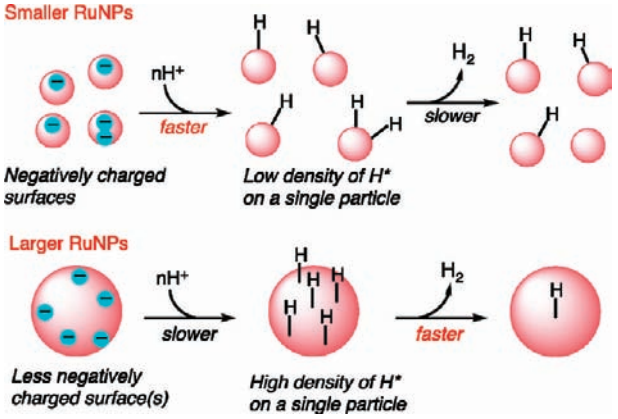

using RuNPs with sizes of 1.1−2.9 nm.[49] The catalytic reactivity increased with the size of the RuNPs, although the selectivity with respect to the partially hydrogenated compound, cyclohexene, decreased.[49] In our system, 4.1 nm RuNPs exhibited the highest specific hydrogen-evolution rate without an increase in the electron-transfer rate. The 4.1 nm RuNPs showed 2-fold higher rates than the 2.1 nm RuNPs.

Size-dependent catalysis by PtNPs has been reported for a photocatalytic hydrogen-evolution system using $[Ru(bpy)_3]^{2+}$, methyl viologen, and triethanolamine as the photosensitizer, electron relay, and sacrificial electron donor, respectively. A previous report concluded that the smaller particles are advantageous both for mass transport of the electroactive species and surface area per gram of catalyst.[50] On the other hand, another research group suggested that a particle size of 3 nm is necessary for the PtNPs to be simultaneously attacked by two molecules of the electron donor and to reserve two electrons for some time until the electrons can be transferred from the particles to two protons on the PtNPs surface to generate a hydrogen molecule.[51] In the current system with RuNPs, the optimum size for hydrogen evolution was 4.1 nm, even though the electron-transfer rates from $QuPh^{\bullet}$−NA to the RuNPs were comparable for RuNPs with different sizes.

As a reaction mechanism for hydrogen evolution, the Volmer−Tafel mechanism has been proposed for electrocatalytic hydrogen evolution with ruthenium electrodes.[52] The mechanism includes two steps of "proton reduction" ($H^+ + e^- \rightarrow H^*$, in which H* is the H adsorbed over the ruthenium electrode) and "hydrogen-atom association" ($2H^* \rightarrow H_2$), where the former and latter steps are denoted as the Volmer and Tafel steps, respectively. In a sulfuric acid solution at room temperature, the Tafel step and consecutive diffusion of H_2 have been reported as rate-determining steps.

As indicated in Figure 7, electron transfer from $QuPh^{\bullet}$−NA to RuNPs is much faster than hydrogen evolution, so the rate-determining step of the photocatalytic hydrogen evolution should come after the electron-transfer step (i.e., the "proton reduction" or "hydrogen-atom association" step). As for "proton reduction" on the surfaces of RuNPs, the proton reduction proceeds faster at smaller RuNPs because the negative charge of the received electron is delocalized over the whole body of the RuNP. Thus, the surfaces of smaller RuNPs are more negatively charged than the surfaces of larger RuNPs. The smaller RuNPs can readily interact with positively charged protons. On the contrary, as for the "hydrogen-atom association" step, larger particles may be advantageous because larger particles can receive more electrons and hydrogen atoms on a single particle than smaller particles, as Toshima et al.[51] proposed for photocatalytic hydrogen evolution by colloidal Pt. Scheme 3 depicts the size effects of the RuNPs on the reaction rates for the "proton reduction" and "hydrogen-atom association" steps. The present results, in which 4.1 nm RuNPs exhibited the highest hydrogen-evolution rate, may be due to well-balanced conditions for both the "proton reduction" and "hydrogen-atom association" steps.

CONCLUSION

Ru nanoparticles have been found to act as efficient hydrogen-evolution catalysts with catalytic reactivity comparable to that of Pt nanoparticles in a photocatalytic hydrogen-evolution system composed of NADH as the electron donor, 2-phenyl-4-(1-naphthyl)-quinolinium ion ($QuPh^+$−NA) as the photocatalyst, and metal nanoparticles (MNPs, M = Pt, Ru) as the hydrogen-evolution catalyst under highly basic conditions around pH 10. The driving force for water oxidation with photogenerated $QuPh^+$−$NA^{+\bullet}$ at pH 10 is as large as 568 kJ mol^{-1}, as calculated from the standard potential for water, E° = 1.229 V vs NHE (which is shifted to 0.639 V vs NHE at pH 10), and the one-electron reduction potential of $QuPh^+$−$NA^{+\bullet}$ (E_{red} = 2.11 V vs NHE in MeCN)[13a] (see page S9 in the SI). The high catalytic reactivity of RuNPs for hydrogen evolution under basic conditions results from the strong reducing ability of $QuPh^{\bullet}$−NA, the one-electron-reduced form of $QuPh^+$−NA, which is generated via photoinduced reduction by NADH. The electron-transfer rates from $QuPh^{\bullet}$−NA to RuNPs were found to be independent of the size of the RuNPs at the same weight, whereas the specific hydrogen-evolution rate normalized by the catalyst weight became maximum for 4.1 nm RuNPs. This is the first example of an efficient photocatalytic hydrogen-evolution system with Ru metal particles working under highly basic conditions by using size-controlled RuNPs as hydrogen-evolution catalysts, providing an excellent opportunity to be combined with water oxidation catalysts.

ASSOCIATED CONTENT

Supporting Information. Time profiles of the decay of the absorption at 420 nm due to $QuPh^{\bullet}$−NA in electron transfer from $QuPh^{\bullet}$−NA to MNPs (M = Ru, Pt, Fe) (Figure S1); time course of hydrogen evolution in a repetitive test (Figure S2); UV−vis absorption of $QuPh^+$−NA and time course of hydrogen evolution under visible-light irradiation (Figure S3); time decay curves of $QuPh^{\bullet}$−NA in MeCN and in a mixed solution of MeCN and H_2O used for quantum yield determination (Figure S4); X-ray diffraction patterns of RuNPs (Figure S5); dynamic laser scattering for determination of the size distribution of RuNPs (Figure S6); time course of hydrogen evolution under photoirradiation using lower concentrations of RuNPs with different sizes (Figure S7); and procedure for calculating the number of RuNPs. This material is available free of charge via the Internet at http://pubs.acs.org.

AUTHOR INFORMATION

Corresponding Author
fukuzumi@chem.eng.osaka-u.ac.jp

■ ACKNOWLEDGMENT

This work was supported by Grants-in-Aid (20108010 and 23750014) and a Global COE Program, "The Global Education and Research Center for Bio-Environmental Chemistry", from the Ministry of Education, Culture, Sports, Science and Technology, Japan (to S.F.) and NRF/MEST of Korea through the WCU (R31-2008-000-10010-0) and GRL (2010-00353) Programs (to S.F.). We sincerely acknowledge the Research Center for Ultra-Precision Science & Technology, Osaka University, for TEM measurements.

■ REFERENCES

(1) (a) Dunn, S. *Encyclopedia of Energy*; Elsevier: Amsterdam, 2004; Vol. 3, p 241. (b) Momirlan, M.; Veziroglub, T. N. *Int. J. Hydrogen Energy* **2005**, *30*, 795.

(2) Laurenczy, G. *Encyclopedia of Catalysis*; Horvath, I. T., Ed.; Wiley-Interscience: Hoboken, NJ, 2010.

(3) (a) Gray, H. B. *Nat. Chem.* **2009**, *1*, 7. (b) Lewis, N. S.; Nocera, D. G. *Proc. Natl. Acad. Sci. U.S.A.* **2006**, *103*, 15729. (c) Nocera, D. G. *Chem. Soc. Rev.* **2009**, *38*, 13.

(4) (a) Grätzel, M. *Acc. Chem. Res.* **1981**, *14*, 376. (b) Kiwi, J.; Kalyanasundaram, K.; Grätzel, M. *Struct. Bonding (Berlin)* **1982**, *49*, 37.

(5) (a) Chan, S. F.; Chou, M.; Creutz, C.; Matsubara, T.; Sutin, N. *J. Am. Chem. Soc.* **1981**, *103*, 369. (b) Darwent, J. R.; Douglas, P.; Harriman, A.; Porter, G.; Richoux, M. C. *Coord. Chem. Rev.* **1982**, *44*, 83. (c) Handman, J.; Harriman, A.; Porter, G. *Nature* **1984**, *307*, 534. (d) Kalyanasundaram, K. *Coord. Chem. Rev.* **1982**, *46*, 159. (e) Krishnan, C. V.; Brunschwig, B. S.; Creutz, C.; Sutin, N. *J. Am. Chem. Soc.* **1985**, *107*, 2005.

(6) (a) Toshima, N. *Pure Appl. Chem.* **2000**, *72*, 317. (b) Toshima, N.; Hirakawa, K. *Polym. J.* **1999**, *31*, 1127.

(7) Jiang, D. L.; Choi, C. K.; Honda, K.; Li, W. S.; Yuzawa, T.; Aida, T. *J. Am. Chem. Soc.* **2004**, *126*, 12084.

(8) (a) Amao, Y. *ChemCatChem* **2011**, *3*, 458. (b) Himeshima, N.; Amao, Y. *Energy Fuels* **2003**, *17*, 1641. (c) Persaud, L.; Bard, A. J.; Campion, A.; Fox, M. A.; Mallouk, T. E.; Webber, S. E.; White, J. M. *J. Am. Chem. Soc.* **1987**, *109*, 7309.

(9) (a) Rau, S.; Schafer, B.; Gleich, D.; Anders, E.; Rudolph, M.; Friedrich, M.; Gorls, H.; Henry, W.; Vos, J. G. *Angew. Chem., Int. Ed.* **2006**, *45*, 6215. (b) Tschierlei, S.; Karnahl, M.; Presselt, M.; Dietzek, B.; Guthmuller, J.; Gonzalez, L.; Schmitt, M.; Rau, S.; Popp, J. *Angew. Chem., Int. Ed.* **2010**, *49*, 3981.

(10) (a) Zhang, X. J.; Jin, Z. L.; Li, Y. X.; Li, S. B.; Lu, G. X. *J. Phys. Chem. C* **2009**, *113*, 2630. (b) Grätzel, M.; Moser, J. *Proc. Natl Acad. Sci. U.S.A.* **1983**, *80*, 3129.

(11) (a) Ozawa, H.; Sakai, K. *Chem. Commun.* **2011**, *47*, 2227. (b) Sakai, K.; Ozawa, H. *Coord. Chem. Rev.* **2007**, *251*, 2753.

(12) (a) Esswein, A. J.; Nocera, D. G. *Chem. Rev.* **2007**, *107*, 4022. (b) Sun, L. C.; Akermark, B.; Ott, S. *Coord. Chem. Rev.* **2005**, *249*, 1653. (c) Wang, M.; Na, Y.; Gorlov, M.; Sun, L. *Dalton Trans.* **2009**, 6458.

(13) (a) Kotani, H.; Ohkubo, K.; Fukuzumi, S. *Faraday Discuss.* [Online early access]. DOI: 10.1039/C1FD00084E. Published Online: July 6, 2011. (b) Kotani, H.; Ohkubo, K.; Takai, Y.; Fukuzumi, S. *J. Phys. Chem. B* **2006**, *110*, 24047. (c) Kotani, H.; Ono, T.; Ohkubo, K.; Fukuzumi, S. *Phys. Chem. Chem. Phys.* **2007**, *9*, 1487.

(14) Harinipriya, S.; Sangaranarayanan, M. V. *Langmuir* **2002**, *18*, 5572.

(15) (a) Dempsey, J. L.; Winkler, J. R.; Gray, H. B. *J. Am. Chem. Soc.* **2010**, *132*, 1060. (b) Dempsey, J. L.; Winkler, J. R.; Gray, H. B. *J. Am. Chem. Soc.* **2010**, *132*, 16774. (c) Dempsey, J. L.; Brunschwig, B. S.; Winkler, J. R.; Gray, H. B. *Acc. Chem. Res.* **2009**, *42*, 1995.

(16) (a) Du, P. W.; Knowles, K.; Eisenberg, R. *J. Am. Chem. Soc.* **2008**, *130*, 12576. (b) Lazarides, T.; Mccormick, T.; Du, P. W.; Luo, G. G.; Lindley, B.; Eisenberg, R. *J. Am. Chem. Soc.* **2009**, *131*, 9192.

(17) Hu, X. L.; Brunschwig, B. S.; Peters, J. C. *J. Am. Chem. Soc.* **2007**, *129*, 8988.

(18) (a) Hinnemann, B.; Moses, P. G.; Bonde, J.; Jorgensen, K. P.; Nielsen, J. H.; Horch, S.; Chorkendorff, I.; Nørskov, J. K. *J. Am. Chem. Soc.* **2005**, *127*, 5308. (b) Karunadasa, H. I.; Chang, C. J.; Long, J. R. *Nature* **2010**, *464*, 1329.

(19) Yagi, T. *J. Biochem.* **1970**, *68*, 649.

(20) Nicolet, Y.; Piras, C.; Legrand, P.; Hatchikian, C. E.; Fontecilla-Camps, J. C. *Structure* **1999**, *7*, 13.

(21) Evans, D. J.; Pickett, C. J. *Chem. Soc. Rev.* **2003**, *32*, 268.

(22) Fontecilla-Camps, J. C.; Volbeda, A.; Cavazza, C.; Nicolet, Y. *Chem. Rev.* **2007**, *107*, 4273.

(23) Darensbourg, M. Y.; Lyon, E. J.; Smee, J. J. *Coord. Chem. Rev.* **2000**, *206*, 533.

(24) Kubas, G. J. *Chem. Rev.* **2007**, *107*, 4152.

(25) (a) Okura, I. *Coord. Chem. Rev.* **1985**, *68*, 53. (b) Okura, I.; Kimthuan, N. *J. Mol. Catal.* **1979**, *6*, 227. (c) Okura, I.; Takeuchi, M.; Kimthuan, N. *Photochem. Photobiol.* **1981**, *33*, 413.

(26) (a) Amao, Y.; Tomonou, Y.; Ishikawa, Y.; Okura, I. *Int. J. Hydrogen Energy* **2002**, *27*, 621. (b) Amao, Y.; Tomonou, Y.; Okura, I. *Sol. Energy Mater. Sol. Cells* **2003**, *79*, 103.

(27) Badura, A.; Esper, B.; Ataka, K.; Grunwald, C.; Woll, C.; Kuhlmann, J.; Heberle, J.; Rogner, M. *Photochem. Photobiol.* **2006**, *82*, 1385.

(28) (a) Krassen, H.; Ott, S.; Heberle, J. *Phys. Chem. Chem. Phys.* **2011**, *13*, 47. (b) Krassen, H.; Schwarze, A.; Friedrich, B.; Ataka, K.; Lenz, O.; Heberle, J. *ACS Nano* **2009**, *3*, 4055.

(29) Kotani, H.; Hanazaki, R.; Ohkubo, K.; Yamada, Y.; Fukuzumi, S. *Chem.—Eur. J.* **2011**, *17*, 2777.

(30) Amouyal, E.; Koffi, P. *J. Photochem.* **1985**, *29*, 227.

(31) Cook, T. R.; Dogutan, D. K.; Reece, S. Y.; Surendranath, Y.; Teets, T. S.; Nocera, D. G. *Chem. Rev.* **2010**, *110*, 6474.

(32) (a) Kleijn, J. M.; Boschloo, G. K. *J. Electroanal. Chem.* **1991**, *300*, 595. (b) Kleijn, J. M.; Lyklema, J. *Colloid Polym. Sci.* **1987**, *265*, 1105. (c) Kleijn, M.; Van Leeuwen, H. P. *J. Electroanal. Chem. Interfacial Electrochem.* **1988**, *247*, 253. (d) Chen, L. L.; Guay, D.; Lasia, A. *J. Electrochem. Soc.* **1996**, *143*, 3576. (e) Spătaru, N.; Helloco, J.-G.; Durand, R. *J. Appl. Electrochem.* **1996**, *26*, 397.

(33) (a) Vijh, A. K.; Belanger, G.; Jacques, R. *Int. J. Hydrogen Energy* **1990**, *15*, 789. (b) Lister, T. E.; Tolmachev, Y. V.; Chu, Y.; Cullen, W. G.; You, H.; Yonco, R.; Nagy, Z. *J. Electroanal. Chem.* **2003**, *554*, 71. (c) Fachinotti, E.; Guerrini, E.; Tavares, A. C.; Trasatti, S. *J. Electroanal. Chem.* **2007**, *600*, 103. (d) Cheng, J.; Zhang, H.; Ma, H.; Zhong, H.; Zou, Y. *Electrochim. Acta* **2010**, *55*, 1855. (e) Amouyal, E.; Keller, P.; Moradpour, A. *J. Chem. Soc., Chem. Commun.* **1980**, 1019.

(34) Greeley, J.; Jaramillo, T. F.; Bonde, J.; Chorkendorff, I.; Nørskov, J. K. *Nat. Mater.* **2006**, *5*, 909.

(35) Ogo, S.; Kabe, R.; Uehara, K.; Kure, B.; Nishimura, T.; Menon, S. C.; Harada, R.; Fukuzumi, S.; Higuchi, Y.; Ohhara, T.; Tamada, T.; Kuroki, R. *Science* **2007**, *316*, 585.

(36) (a) Viau, G.; Brayner, R.; Poul, L.; Chakroune, N.; Lacaze, E.; Fiévet-Vincent, F.; Fiévet, F. *Chem. Mater.* **2003**, *15*, 486. (b) Yan, X.; Liu, H.; Liew, K. Y. *J. Mater. Chem.* **2001**, *11*, 3387.

(37) Peng, S.; Wang, C.; Xie, J.; Sun, S. H. *J. Am. Chem. Soc.* **2006**, *128*, 10676.

(38) (a) Gärtner, F.; Boddien, A.; Barsch, E.; Fumino, K.; Losse, S.; Junge, H.; Hollmann, D.; Bruckner, A.; Ludwig, R.; Beller, M. *Chem.—Eur. J.* **2011**, *17*, 6425. (b) Gärtner, F.; Sundararaju, B.; Surkus, A. E.; Boddien, A.; Loges, B.; Junge, H.; Dixneuf, P. H.; Beller, M. *Angew. Chem., Int. Ed.* **2009**, *48*, 9962.

(39) (a) Zhang, P.; Wang, M.; Dong, J.; Li, X.; Wang, F.; Wu, L.; Sun, L. *J. Phys. Chem. C* **2010**, *114*, 15868. (b) Zhang, P.; Wang, M.; Na, Y.; Li, X.; Jiang, Y.; Sun, L. *Dalton Trans.* **2010**, *39*, 1204.

(40) Anderson, J. R. *Structure of Metallic Catalysts*; Academic Press: London, 1975.

(41) Fukuzumi, S.; Kotani, H.; Ohkubo, K. *Phys. Chem. Chem. Phys.* **2008**, *10*, 5159.

(42) (a) Fukuzumi, S.; Tanaka, T. In *Photoinduced Electron Transfer, Part C*; Fox, M. A., Chanon, M., Eds.; Elsevier: Amsterdam, 1988. (b) Zhu, X. Q.; Yang, Y.; Zhang, M.; Cheng, J. P. *J. Am. Chem. Soc.* **2003**, *125*, 15298.

(43) Fukuzumi, S.; Miyao, H.; Ohkubo, K.; Suenobu, T. *J. Phys. Chem. A* **2005**, *109*, 3285.
(44) (a) Fukuzumi, S.; Inada, O.; Suenobu, T. *J. Am. Chem. Soc.* **2002**, *124*, 14538. (b) Fukuzumi, S.; Inada, O.; Suenobu, T. *J. Am. Chem. Soc.* **2003**, *125*, 4808.
(45) (a) Fukuzumi, S.; Noura, S. *J. Chem. Soc., Chem. Commun.* **1994**, 287. (b) Fukuzumi, S.; Fujita, M.; Noura, S.; Ohkubo, K.; Suenobu, T.; Araki, Y.; Ito, O. *J. Phys. Chem. A* **2001**, *105*, 1857.
(46) (a) Yoon, U. C.; Quillen, S. L.; Mariano, P. S.; Swanson, R.; Stavinoha, J. L.; Bay, E. *J. Am. Chem. Soc.* **1983**, *105*, 1204. (b) Nishimine, M.; Ohkubo, K.; Komori, T.; Fukuzumi, S. *Chem. Commun.* **2003**, 1886.
(47) Ohkubo, K.; Mizushima, K.; Iwata, R.; Souma, K.; Suzuki, N.; Fukuzumi, S. *Chem. Commun.* **2010**, *46*, 601.
(48) Joo, S. H.; Park, J. Y.; Renzas, J. R.; Butcher, D. R.; Huang, W.; Somorjai, G. A. *Nano Lett.* **2010**, *10*, 2709.
(49) Campbell, P. S.; Santini, C. C.; Bayard, F.; Chauvin, Y.; Collière, V.; Podgoršek, A.; Costa Gomes, M. F.; Sá, J. *J. Catal.* **2010**, *275*, 99.
(50) Kiwi, J.; Grätzel, M. *J. Am. Chem. Soc.* **1979**, *101*, 7214.
(51) Toshima, N.; Kuriyama, M.; Yamada, Y.; Hirai, H. *Chem. Lett.* **1981**, 793.
(52) Breiter, M. W. *J. Electroanal. Chem. Interfacial Electrochem.* **1984**, *178*, 53.